Japanese Journal of Applied Physics **53**, 07KF02 (2014) **BRIEF NOTE**
http://dx.doi.org/10.7567/JJAP.53.07KF02

Comparison of spatial resolutions of parallel beamforming and diffraction tomography in high frame rate echocardiography

Hideyuki Hasegawa[1,2] and Hiroshi Kanai[1,2*]

[1]*Graduate School of Biomedical Engineering, Tohoku University, Sendai 980-8579, Japan*
[2]*Graduate School of Engineering, Tohoku University, Sendai 980-8579, Japan*
E-mail: hasegawa@ecei.tohoku.ac.jp

Received November 28, 2013; accepted March 5, 2014; published online June 4, 2014

Echocardiography is a predominant modality for diagnosis of the heart by noninvasive and real-time observation of its cross-sectional images. In addition, it has been recently shown that measurement of the rapid transition of myocardial contraction/relaxation and propagation of heart-wall vibration would be useful for assessment of myocardial function and viscoelasticity. However, such measurements require a higher frame rate of several hundred hertz. Therefore, we realized high-frame-rate echocardiography using parallel beamforming with unfocused transmit beams. On the other hand, there is another imaging method, namely, diffraction tomography. It has been reported that diffraction tomography realizes high spatial resolution. One of the problems of parallel beamforming with unfocused transmit beams is the degradation of spatial resolution; diffraction tomography may alleviate this problem. In the present study, diffraction tomography was applied to high-frame-rate echocardiography with unfocused transmit beams, and spatial resolutions realized by diffraction tomography and parallel beamforming were compared. Diffraction tomography showed a spatial resolution (1.16 mm) similar to that (1.18 mm) of parallel beamforming in a relatively near region (44 mm in range distance). In a deeper region (84 mm), diffraction tomography realized better spatial resolution (1.90 mm) than that (2.27 mm) of parallel beamforming. However, still better spatial resolution (1.57 mm) was realized by parallel beamforming when it was used with a phase coherence factor. The use of the phase coherence factor is not computationally intensive, and parallel beamforming with a phase coherence factor was shown to be feasible in high-frame-rate echocardiography for the improvement of spatial resolution.

Recently, it has been reported that the propagation of electrical stimulation and spontaneous vibration of heart muscle could be used for the evaluation of myocardial viscoelasticity and viability.[1,2)] For the measurement of such propagation phenomena, higher temporal resolution of several hundreds of hertz is necessary because the propagation speed is relatively high (up to several m/s).[3)] Also, it has been shown that high-frame-rate echocardiography is useful for the evaluation of myocardial function.[4–6)]

Various studies have been conducted on increasing the frame rate. Konofagou et al.[7)] and D'hooge et al.[8)] increased the frame rate to above 200 Hz by reducing the size of the field of view and the total number of scan lines in an ultrasonic image. Furthermore, Konofagou et al. introduced an electrocardiogram (ECG)-gating technique in ultrasound imaging to combine individual small sectors into a large field of view.[9)] In this method, the lateral size of a sector (corresponding to the number of scan lines), which is obtained in one acquisition, is narrowed to achieve a higher frame rate of about 500 Hz. By measuring a number of small sectors during the corresponding number of cardiac cycles, the measured small sectors are combined into a large sector format based on the ECG-gating. Although this method achieves a frame rate of about 500 Hz, which is much higher than the conventional frame rate of several tens of hertz, measurements for a number of cardiac cycles are required.

To obtain the number of scan lines required to construct a B-mode image with fewer transmissions, parallel beamforming has been proposed.[10)] Recently, parallel beamforming with plane-wave transmissions has been intensively used in transient elastography[11)] with a linear array probe. However, in echocardiography, the size of the aperture is very limited because it is necessary to insonify ultrasound from a narrow acoustic window between ribs. To solve this problem, we realized high-frame-rate echocardiography by parallel beamforming with diverging wave transmissions, and an ultrasound image of the heart with a full lateral field of view of 90 degrees was obtained at a very high frame rate of 316 Hz.[12,13)]

On the other hand, there is another imaging method, namely, diffraction tomography,[14,15)] which is reported to yield ultrasound images with high spatial resolution. In the present study, spatial resolutions of parallel beamforming (PBF) and diffraction tomography (DT) were examined for the improvement of spatial resolution in high-frame-rate echocardiography with unfocused transmit beams.

Currently, DT can be used with plane-wave transmission[15,16)] or synthetic aperture imaging.[14)] To use DT with diverging wave transmission, a diverging wave must be assumed to be a plane wave. Consequently, the diverging angle should be less than 15 degrees, but images obtained by DT with diverging beams were degraded compared with those obtained by DT with plane waves.[17)] Therefore, in the present study, spatial resolutions of PBF and DT were compared using a single plane-wave transmission.

In parallel receive beamforming,[12,13)] ultrasound echo signals $\{s_i(t)\}$ received by individual transducer elements are summed after applying appropriate delays depending on the relative geometry between each element i ($i = 0, 1, ..., L-1$) and a point of interest $\mathbf{p} = (r, \theta)$. The time delay $\tau_i(\mathbf{p})$ applied to the signal received by the i-th transducer element is expressed as

$$\tau_i(\mathbf{p}) = \tau_{\mathrm{tr}}(\mathbf{p}) + \frac{1}{c_0}\left[r^2\cos^2\theta + \left\{r\sin\theta - \Delta x\left(i - \frac{L-1}{2}\right)\right\}^2\right]^{0.5}, \quad (1)$$

where c_0 is the speed of sound and $\tau_{\mathrm{tr}}(\mathbf{p})$ is the propagation time delay of a transmit beam from the transducer array to the point of interest $\mathbf{p}$. In the case of plane-wave transmission, $\tau_{\mathrm{tr}}(\mathbf{p})$ is expressed as

$$\tau_{\mathrm{tr}}(\mathbf{p}) = \frac{r\cos(\theta - \Theta)}{c_0}, \quad (2)$$

where Θ is the direction of the transmit beam.

The beamformed RF signal $g(\mathbf{p})$ at spatial point $\mathbf{p}$ is obtained as

$$g(\mathbf{p}) = \sum_{0}^{L-1} s(t - \tau_i(\mathbf{p})). \quad (3)$$

Let us briefly describe the principle of diffraction tomography with plane-wave transmission.[16] Assuming the scattering coefficient $\gamma(x,z)$ at spatial point $\mathbf{p} = (r,\theta) = (x,z)$ depends on the local fluctuation of the bulk modulus and using Born approximation, echo signal $s(x_m,\omega)$ scattered at point $\mathbf{p} = (x,z)$ and received at position $\mathbf{p}_m = (x_m, 0)$ of the m-th transducer element is expressed as

$$s(x_m,\omega) = k^2 \iint_{-\infty}^{\infty} p_i(\mathbf{p}) \cdot \gamma(\mathbf{p}) \cdot g(\mathbf{p}_m|\mathbf{p})\, dx\, dz, \quad (4)$$

where k is the wavenumber ($= \omega/c_0$, ω: angular frequency).

In the present study, a plane wave was used as the transmitted wave $p_i(\mathbf{p})$. A plane wave propagating in the direction (q_x, q_z) is expressed as

$$p_i(\mathbf{p}) = A \cdot \exp\{j(q_x x + q_z z)\}, \quad (5)$$

where A is an amplitude coefficient. Assuming the scattered wave from point $\mathbf{p}$ is a circular wave, which is expressed by the Hankel function of the first kind of order 0, the Green function $g(\mathbf{p}_m|\mathbf{p})$ is expressed as

$$\begin{aligned} g(\mathbf{p}_m|\mathbf{p}) &= H_0^{(1)}(k|\mathbf{p}_m - \mathbf{p}) \\ &= \frac{j}{4\pi} \int_{-\infty}^{\infty} \frac{\exp[j\{k_x(x_m - x) - \sqrt{k^2 - k_x^2}z\}]}{\sqrt{k^2 - k_x^2}}\, dk_x, \end{aligned} \quad (6)$$

where k_x is the wavenumber in the x-direction. Equation (4) can be modified as

$$\begin{aligned} s(x_m,\omega) = \frac{jk^2A}{4\pi} \iint_{-\infty}^{\infty} \gamma(x,z) \cdot \exp\{j(q_x x + q_z z)\} \\ \times \int_{-\infty}^{\infty} \frac{\exp[j\{u(x_m - x) - \sqrt{k^2 - u^2}z\}]}{\sqrt{k^2 - u^2}}\, du\, dx\, dz. \end{aligned} \quad (7)$$

By applying the Fourier transform to $s(x_m,\omega)$ with respect to x_m, the 2-D frequency spectrum $S(k_x,\omega)$ of echo signals received by individual transducer elements is expressed as

$$\begin{aligned} S(k_x,\omega) &= \int_{-\infty}^{\infty} s(x_m,\omega) \cdot \exp(-jk_x x_m)\, dx_m \\ &= \frac{jk^2A}{4\pi} \iint_{-\infty}^{\infty} \gamma(x,z) \cdot \exp\{j(q_x x + q_z z)\} \\ &\quad \times \int_{-\infty}^{\infty} \frac{\exp\{-j(ux + \sqrt{k^2 - u^2}z)\}}{\sqrt{k^2 - u^2}} \\ &\quad \times \int_{-\infty}^{\infty} \exp\{j(u - k_x)x_m\}\, dx_m\, du\, dx\, dz. \end{aligned} \quad (8)$$

Using Dirac's delta function $\delta(\cdot)$

$$\int_{-\infty}^{\infty} \exp\{-j(k_x - u)x_m\}\, dx_m = 2\pi\delta(k_x - u), \quad (9)$$

Equation (8) is modified as

$$\begin{aligned} S(k_x,\omega) = \frac{jk^2A}{2} \iint_{-\infty}^{\infty} \gamma(x,z) \cdot \exp\{j(q_x x + q_z z)\} \\ \times \frac{\exp\{-j(k_x x + \sqrt{k^2 - k_x^2}z)\}}{\sqrt{k^2 - k_x^2}}\, dx\, dz \end{aligned}$$

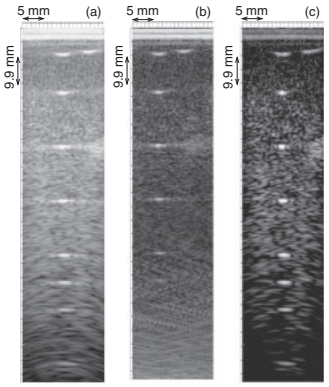

Fig. 1. B-mode images of phantom obtained by (a) parallel beamforming, (b) diffraction tomography, and (c) parallel beamforming with phase coherence factor.

$$= \frac{jk^2A}{2\sqrt{k^2 - k_x^2}} \iint_{-\infty}^{\infty} \gamma(x,z) \times \exp[-j\{(k_x - q_x)x + (\sqrt{k^2 - k_x^2} - q_z)z\}]\, dx\, dz. \quad (10)$$

The right-hand side of Eq. (10) corresponds to the 2-D frequency spectrum $\Gamma(k_x - q_x, (k^2 - k_x^2)^{1/2} - q_x)$ of the scattering coefficient distribution $g(x,z)$. Therefore, Eq. (10) is expressed as

$$S(k_x,\omega) = j\frac{k^2A}{2\sqrt{k^2 - k_x^2}} \cdot \Gamma(k_x - q_x, \sqrt{k^2 - k_x^2} - q_x). \quad (11)$$

By applying the inverse Fourier transform to Eq. (11), the scattering coefficient distribution $g(x,z)$ is estimated.

An ultrasound imaging phantom (CIRS 54GS) was measured using modified ultrasonic diagnostic equipment (Hitachi-Aloka α-10) with a 3.75 MHz phased array probe. Ultrasonic echoes received by individual transducer elements were acquired at a sampling frequency of 30 MHz at a 12-bit resolution.

Spatial resolutions of PBF and DT were compared by constructing B-mode images from one transmission of a plane wave at a steering angle of 0°. Figures 1(a) and 1(b) show B-mode images of the phantom obtained by PBF and DT, respectively. Lateral amplitude profiles at wire strings located at range distances of 44, 64, and 84 mm are shown in Figs. 2(a)–2(c). Only in Fig. 2(1-a), lateral amplitude profiles obtained by rectangular (red) and Hamming (green) receive apodization are shown. By comparing Figs. 2(1-b) and 2 (2-b), we found that the amplitude profile obtained by DT corresponds to that obtained by PBF with rectangular receive apodization. Therefore, lateral amplitude profiles obtained by PBF with rectangular receive apodization were compared with those obtained by DT. As can be seen from the full widths at half-maximum of the amplitude profiles listed in Table I, spatial resolutions of PBF and DT are similar in a shallow region (44 mm), but the spatial resolution of DT is slightly better than that of PBF in deeper regions. In DT, Eq. (11) is calculated for each frequency component contained in the received ultrasonic echo signal by Fourier transform. After the calculation of Eq. (11), all the acquired frequency components are combined by inverse Fourier transform. Therefore, DT can utilize the frequency band of

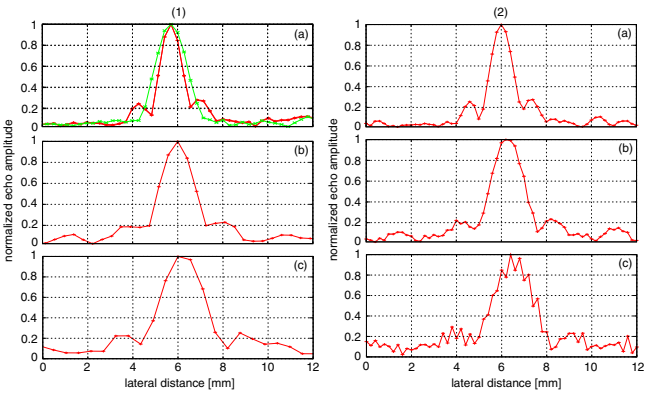

Fig. 2. (Color online) Results obtained by (1) parallel beamforming and (2) diffraction tomography. Lateral amplitude profiles (red: rectangular receive apodization, green: Hamming receive apodization) at (a) 44, (b) 64, and (c) 84 mm.

Table I. Lateral spatial resolutions of PBF, DT, and PBF with PCF (unit: mm).

	Depth		
	44	64	84
PBF	1.18	1.79	2.27
DT	1.16	1.70	1.90
PBF with PCF	0.79	1.16	1.57

the pulsed ultrasound used for imaging, and a spatial resolution similar to that of PBF can be obtained.

On the other hand, PBF can be used with a weighting method, namely, phase coherence factor (PCF),[18] which evaluates the variance in phases of echo signals received by individual elements after the operation of delay compensation, as in the conventional delay and sum beamforming process. PCF can suppress echoes from scatterers except for that scattered from a focal point. Also, PCF can suppress echo signals with low signal-to-noise ratios (SNRs) because the phases of echo signals with low SNRs tend to fluctuate randomly. The random fluctuation of phase increases the phase variance, and PCF becomes low. As a result, PCF also improves the SNR of the obtained ultrasonic image by suppressing echo signals with low SNRs. PCF can be used with low computational load and would be useful also for the improvement of spatial resolution in PBF. Figure 1(c) shows a B-mode image of the phantom obtained by PBF with PCF, and Fig. 3 shows lateral amplitude profiles at a range distance of 44 mm obtained by PBF, DT, and PBF with PCF. The full widths at half-maximum of the amplitude profiles in Fig. 3 are listed in Table I. As can be seen in Fig. 3, PBF with PCF achieved much better spatial resolution than did PBF and DT. Actually, DT achieved slightly better spatial resolution than PBF, but DT requires the 2-D Fourier transform and inverse 2-D Fourier transform. Although fast Fourier transform can be used for enhancing computational efficiency, PCF does not need a high computational load and, therefore, PBF with PCF would be useful for high temporal and spatial resolution echocardiography. One of the problems in the use of PCF is the suppression of speckle echoes from a diffuse scattering

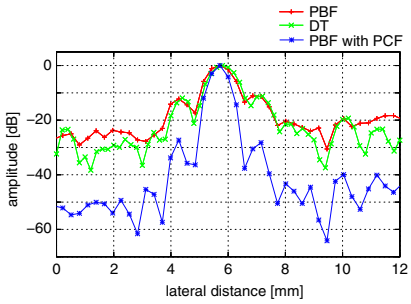

Fig. 3. (Color online) Lateral amplitude profiles at a range distance of 44 mm obtained by the various methods.

medium, such as echoes from the inside of the heart wall. This problem should be solved in future work to enable the use of high-frame-rate echocardiography with PCF.

High-frame-rate echocardiography contributes to the measurement of cardiac dynamics, which must be measured to assess myocardial function and viscoelasticity. In the present study, parallel beamforming and diffraction tomography were examined for the improvement of spatial resolution in high-frame-rate echocardiography using unfocused transmit beams. Diffraction tomography improved the spatial resolution in a deeper region compared with parallel beamforming alone. However, parallel beamforming with the phase coherence factor further improved the spatial resolution. The calculation of the phase coherence factor did not require extensive computational load, and parallel beamforming with the phase coherence factor was considered to be feasible for realizing high temporal and spatial resolution echocardiography.

1) H. Kanai, IEEE Trans. Ultrason. Ferroelectr. Freq. Control **52**, 1931 (2005).
2) H. Kanai and M. Tanaka, Jpn. J. Appl. Phys. **50**, 07HA01 (2011).
3) D. M. Bers, *Excitation-Contraction Coupling and Cardiac Contractile Force* (Kluwer Academic, Dordrecht, 2001) 2nd ed.
4) Y. Honjo, H. Hasegawa, and H. Kanai, Jpn. J. Appl. Phys. **49**, 07HF14 (2010).
5) Y. Honjo, H. Hasegawa, and H. Kanai, Jpn. J. Appl. Phys. **51**, 07GF06 (2012).
6) H. Shida, H. Hasegawa, and H. Kanai, Jpn. J. Appl. Phys. **51**, 07GF05 (2012).
7) E. E. Konofagou, J. D'hooge, and J. Ophir, Ultrasound Med. Biol. **28**, 475 (2002).
8) J. D'hooge, E. Konofagou, F. Jamal, A. Heimdal, L. Barrios, B. Bijnens, J. Thoen, F. van de Werf, G. Sutherland, and P. Suetens, IEEE Trans. Ultrason. Ferroelectr. Freq. Control **49**, 281 (2002).
9) S. Wang, W. Lee, J. Provost, J. Luo, and E. E. Konofagou, IEEE Trans. Ultrason. Ferroelectr. Freq. Control **55**, 2221 (2008).
10) D. P. Shattuck, M. D. Weinshenker, and S. W. Smith, J. Acoust. Soc. Am. **75**, 1273 (1984).
11) M. Tanter, J. Bercoff, L. Sandrin, and M. Fink, IEEE Trans. Ultrason. Ferroelectr. Freq. Control **49**, 1363 (2002).
12) H. Hasegawa and H. Kanai, J. Med. Ultrason. **38**, 129 (2011).
13) H. Hasegawa and H. Kanai, IEEE Trans. Ultrason. Ferroelectr. Freq. Control **59**, 2569 (2012).
14) K. Nagai, IEEE Trans. Sonics Ultrason. **32**, 531 (1985).
15) J. Cheng and J. Lu, IEEE Trans. Ultrason. Ferroelectr. Freq. Control **53**, 880 (2006).
16) P. M. Morse and K. U. Ingard, *Theoretical Acoustics* (Princeton University Press, Princeton, NJ, 1968).
17) J. Lu and H. Chen, Proc. IEEE Int. Ultrasonics Symp., 2011, p. 2221.
18) J. Camacho, M. Parrilla, and C. Fritsch, IEEE Trans. Ultrason. Ferroelectr. Freq. Control **56**, 958 (2009).